Electrochemical Materials and Technologies

ARTICLE

eISSN:2949-0561

Cite this: Electrochem. Mater. Technol. 2 (2023) 20232013

Received: 3 May 2023
Accepted: 1 June 2023
Published online: 9 June 2023

DOI: 10.15826/elmattech.2023.2.013

Studying effects of external conditions of electrochemical measurements on the photoelectrochemical properties of semiconductors: cyclic voltammetry, impedance spectroscopy, and Mott – Schottky method

Dina Markovskaya [a]*, Nikolay Sidorenko [a], Angelina Zhurenok [a], Ekaterina Kozlova [a]

In this paper, the dependences of the semiconductors' photoelectrochemical properties on the experimental conditions were studied for the solid solution of CdS and ZnS, graphitic carbon nitride, and the platinized carbon nitride. The cyclic voltammograms were obtained under different scan rates. The sample investigations were carried out by two ways, at the constant external voltage and varied amplitudes and at different external voltages and the fixed amplitude. The Mott – Schottky dependences were studied at different frequencies. The basic dependences of the changes in the photoelectrode target characteristics on the experimental conditions were found. Some recommendations for the correct comparison of qualitative and quantitative photoelectrochemical data were formulated.

keywords: electrochemical methods, impedance, external voltage, amplitude, Mott – Schottky plot, cyclic voltammetry

1. Introduction

In contemporary society, science faces a lot of questions, one way or another related to the ecological situation of the planet and the gradual depletion of the resources [1–8]. There are rather strict requirements regarding environmental safety for the technologies being developed. The usage of sun light for chemical reactions was attractive because solar energy belonged to inexhaustible resources and did not cause any secondary pollutions [1, 2]. Sun light may be used for the initialization and realization of chemical processes called photocatalytic. Photocatalytic processes find application in solving various tasks such as hydrogen generation [3], reduction of carbon dioxide [4], oxidation of organic compounds [5], cleaning of water [6] and air [7] from impurities, disinfection [8] etc.

The key issue of photocatalysis is the properties of photocatalysts and their relationships with catalytic activity. Currently, photoelectrochemical methods such as voltammetry, impedance spectroscopy, and chronoamperometry are widely used to study photocatalysts. These methods allow one to obtain additional information of the studied systems [9–11]. Voltammetry methods can help with identifying electrochemical processes occurring at the semiconductor surface in the electrolyte and calculating the main photovoltaic characteristics of the cell [9, 10]. Impedance spectroscopy considers the electron transitions into the electrochemical cell and allows

a: Department of heterogeneous catalysis, Boreskov Institute of Catalysis, Novosibirsk 630090, Russia

* Corresponding author: madiva@catalysis.ru

estimating charge carriers lifetime [11, 12]. The chronoamperometry shows the evolution of the current density over time under a constant applied potential to the photoelectrochemical cell. This method may estimate the electrode photostability, using other methods, define the processes causing changes in current density over time. Besides, the photoelectrochemical methods allow one to significantly expand the understanding of the processes occurring during the work of the studied photocatalysts and their corresponding photoelectrodes.

However, there is a problem of the correct comparison of the obtained experimental results with the literature connected with different experimental conditions. In the experiments, the apparatus parameters may be changed, besides using different counter electrodes, electrolytes of varied nature and concentration. In case of voltammetry, the researchers change the range of potentials and scan rate. Studying by the impedance spectroscopy can be carried out at the varied frequencies, external potentials and amplitudes. If we compare the results obtained at different conditions, the questions arise: how do the target parameters change under the experimental conditions, in what cases do the dependences between different series save or do not save, which photoelectrochemical properties obtained under different conditions do compare between each other? Additionally, the Mott – Schottky experiments are conducted at different frequencies, potentials, and amplitude. For example, H. Chen et al. estimated the flat-band potential of *g*-C_3N_4 at frequencies 2000 Hz and 3000 Hz [13] and obtained –1.4 V, while P. Bai et al. measured it in the same solution at frequencies 500 Hz and calculated –1.2 V [14]. Were the differences between these values caused by only the experimental errors? How do the frequencies imply on the flat-band values? Nowadays, there are no published materials about this effect in a wide range of frequencies.

In this work, three samples were studied by photoelectrochemical methods varying different experimental conditions. For the investigations, two response-to-visible-light semiconductors such as the solid solution of cadmium sulfide and zinc sulfide $Cd_{0.8}Zn_{0.2}S$ showed earlier high photoelectrochemical characteristics [15] and graphitic carbon nitride were chosen. Moreover, the platinized *g*-C_3N_4 was tested under the same conditions. In cyclic voltammetry, scan rate from 5 to 100 mV/s was varied; the amplitude (5–100 mV) and external potential (from –0.8 V to 0.8 V) was changed for the impedance spectroscopy while the frequencies ($\lg(f) = 0–5$) differed for the Mott – Schottky dependences. The comprehensive work in which the tested properties examined with photoelectrochemical methods under a wide range of the apparatus parameters carried out for the first time. The features of changing the photovoltaic parameters which were dependent on the scan rate were found for the first time. The trends of changes in the electron lifetime measured at varied external potentials and amplitudes are observed for the first time. Based on the obtained results, some recommendations for the correct comparison of qualitative and quantitative photoelectrochemical data were formulated.

2. Experimental

The solid solution of cadmium sulfide and zinc sulfide $Cd_{0.8}Zn_{0.2}S$ was prepared by the deposition of sulfides from as-prepared zinc hydroxide and cadmium hydroxide sulfides [15]. The carbon nitride was synthesized by melamine calcination at 550 °C for 2 hours. The platinum was deposited by the reduction of hexachloroplatinic acid with excess of sodium borohydride [16].

All photoelectrochemical experiments were carried out on a potentiostat-galvanostat P-45X (Russia) with an electrochemical impedance measurement module FRA-24M under irradiation with a photodiode (λ = 450 nm). All measurements were conducted in a two-electrode electrochemical cell. The FTO substrate with 30 mg of the deposited photocatalyst served as the working electrode. The obtained photoelectrodes were labeled as CZS, CN, and Pt-CN for $Cd_{0.8}Zn_{0.2}S$/FTO, C_3N_4/FTO, and 1 % Pt/C_3N_4, respectively. The brass with deposited Cu_2S was used as the counter electrode. The measurements were carried out in the electrolyte prepared by adding sodium chloride (0.1 M) and sulfur (1 M) to 1 M Na_2S solution. This electrolyte prevents the photocorrosion of the solid solutions of CdS and ZnS [15]. Sodium chloride is added as an additional charge source in the photoelectrochemical cell. Further experiments show that graphitic carbon nitride (with or without deposited platinum) also produces the photocurrent in the cell with this electrolyte. The electrodes were compressed to improve the contacts. The samples were studied by cyclic voltammetry, the potential range was from –0.8 V to 0.8 V, the scan rate was from 5 to 100 mV/s. The potential range was chosen from literature data. The researchers studied cadmium sulfide or graphitic carbon nitride at different potentials such as 0–1 V [17] or –0.6–1 V [18]. In this study, we tested both the negative and the positive regions. The chosen scan rates are often used by other researchers and mentioned in the literature [13, 14]. Scan rates that are lower than 10 mV/s or higher than 100 mV/s are rarely mentioned.

Additionally, the samples were examined by impedance spectroscopy (frequency was changed from 0.8 to 10^5 Hz, amplitude was from 5 to 100 mV at the constant external potential 200 mV or amplitude was 10 mV at the variable potential from –0.8 to 0.8 V), and by the Mott – Schottky method (potential range was from –0.6 V to 0.7 V, amplitude was 10 mV, frequencies were 10^5 Hz, 10^4 Hz, 1000 Hz, 100 Hz, 10 Hz, 1 Hz).

3. Results and discussion

3.1. The effect of the potential sweep rate on the photovoltaic characteristics of a photoelectrochemical cell

For all samples, the cyclic voltammograms were obtained in the potential range from –0.8 to 0.8 V vs the counter electrode at different scan rates (5–100 mV·s^{-1}). Figure 1 shows the first two cycles measured at the scan rates of 20 mV·s^{-1} and 80 mV·s^{-1} for all examined photoelectrodes. The current densities observed at the applied potentials were higher in the presence of the photoelectrode with the deposited graphitic carbon nitride than for the sample with the solid solution of cadmium sulfide and zinc sulfide. This trend remains the same for both scan rates. For the cell with CN as the working electrode, the current density is higher than for the one with CZS; however, the difference between them is greater for the scan rate equal 20 mV·s^{-1}. By the way, the photoelectrode screening is better to conduct at low scan rates, in this region the difference between the electrochemical activities of the analyzed samples is more evident at the quantitative level. However, general trends are revealed at both low and high scan rates.

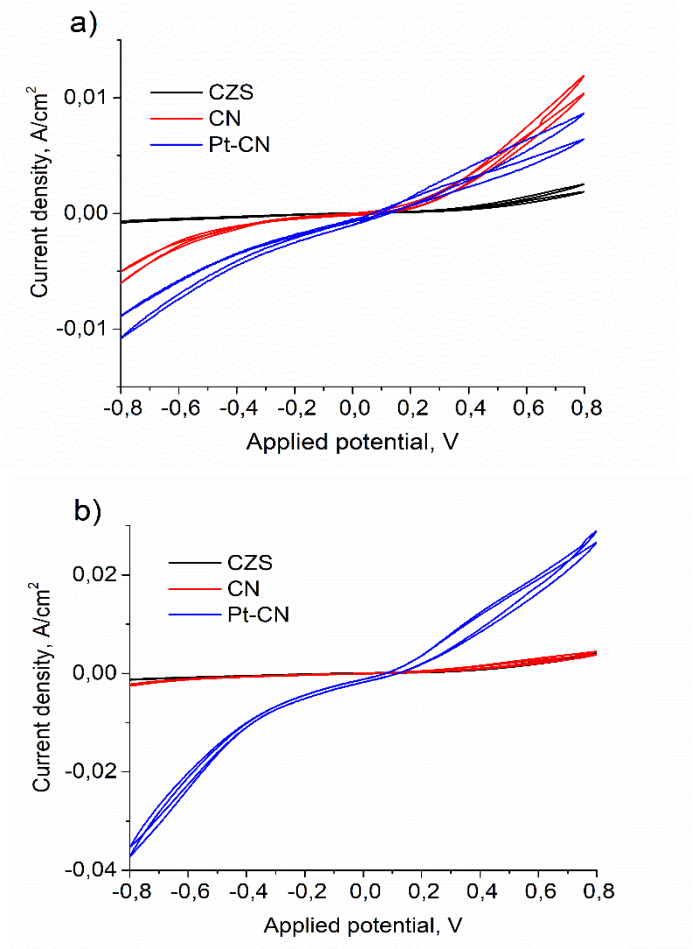

Figure 1 Cyclic voltammograms of CZS, CN, Pt-CN measured at scan rate of a) 20 and b) 80 mV/s.

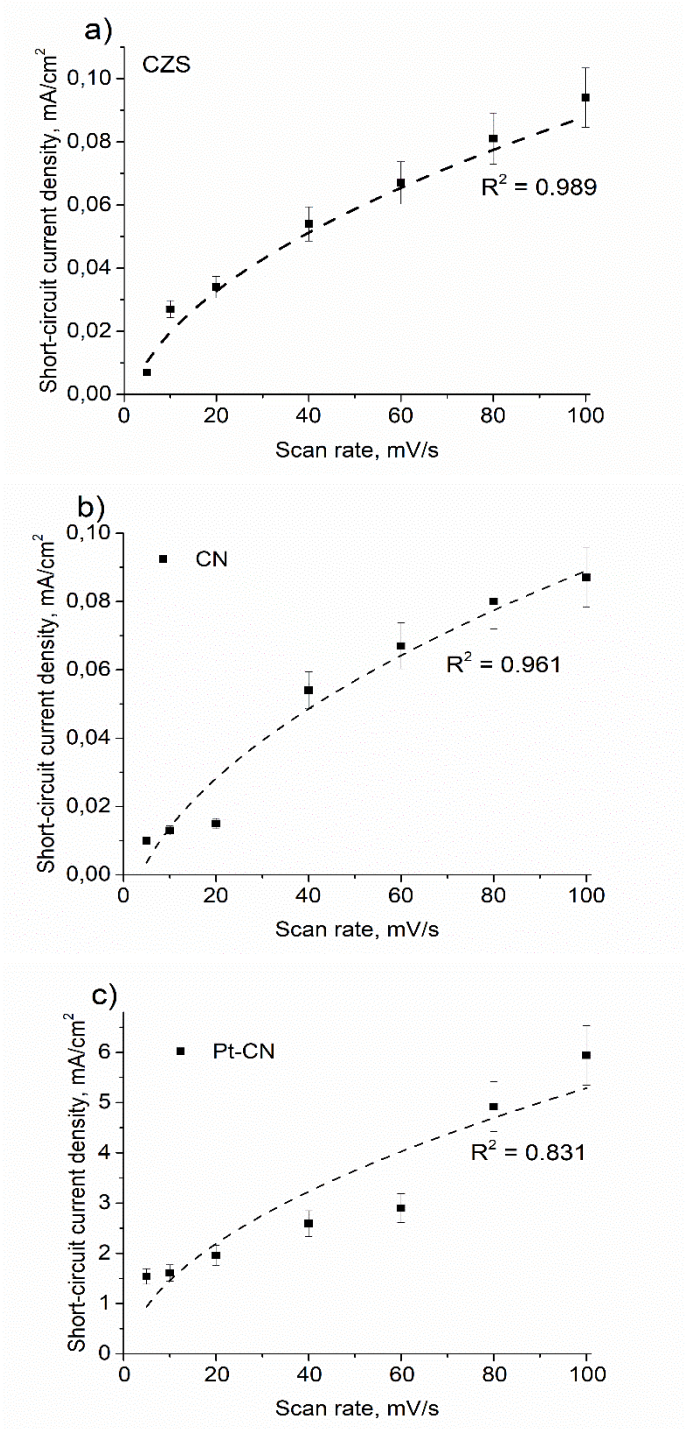

Figure 2 Dependences of short-circuit current density on scan rate obtained in the cell with a) CZS, b) CN, c) Pt-CN photoelectrode. The dotted line shows the data approximation by a power function with a power of 0.5.

From the voltammograms, typical characteristics of the photoelectrochemical cell such as short-circuit current density, open circuit voltage, fill factor, and power conversion efficiency can be calculated. For all samples, these values were calculated from the second cycle when the potential was changed from 0.8 V to –0.8 V, and the obtained values were summed up in Table 1. Table 1 and Figure 2 demonstrate that the short-circuit current density increases in proportion to the square root of the potential scan rate. Moreover, the growth rate for the solid solution of cadmium sulfide and zinc sulfide, and carbon nitride does not differ within the measurement error. Probably, the observed dependency has the same nature as the change in a current maximum during varying potential scan rate described by Randles – Sevcik equation ($I \sim v^{0.5}$). Note that the rate of increase in the short-circuit current density with the growth of the scan rate for Pt-CN is higher than that for carbon nitride by almost one order.

Table 1 shows that the open circuit potential, which is a potential with no current in the photoelectrochemical cell, changes according to the logarithmic law with the growth of the scan rate (see Figure 3a) and reaches a plateau. The obtained dependency is quite expected. It is known that the maximum possible value of the open circuit voltage is logarithmically related to the short-circuit current density (I) [9] whose dependence on the scan rate is described by a power law. Since, when logarithming a power function, the power is taken as the sign of the logarithm, the dependences of the open circuit voltage on the short-circuit current density and the scan rate are logarithmic.

Figure 3b shows the approximations of the dependences of the open circuit voltage on the short circuit current density by the function $y = a + b\ln(x + c)$ for the CN, CZS electrodes. The same dependence for Pt-CN is given in Figure 3c. The found dependence describes the data observed in the experiment with high accuracy.

$$V_{OC} = \frac{n \cdot k_B \cdot T}{e}\left[\ln\frac{I_{sc}}{I_0} + 1\right] \qquad (1)$$

where V_{oc} is the open circuit voltage, n is a diode quality coefficient, k_B is Boltzmann's constant, T is the temperature, e is the electron charge, I_{sc} is short-circuit current, I_0 is saturation current occurring by free charge carriers generated by thermal excitation.

The next parameter describing the photoelectrochemical cell is the fill factor. It shows the effect of ohmic losses on the cell efficiency [9, 10]. Table 1 reveals that the fill factor changes from 24 % to 29 % for CZS and CN, and from 24 % to 26 % for Pt-CN. Therefore, the fill factor does not depend on the scan rate practically. From the physical point of view, this result is expected because the resistance occurring in the photoelectrochemical cell during charge transfer is not connected with the scan rate. The individual values of current and voltage will vary, but their ratio will remain constant.

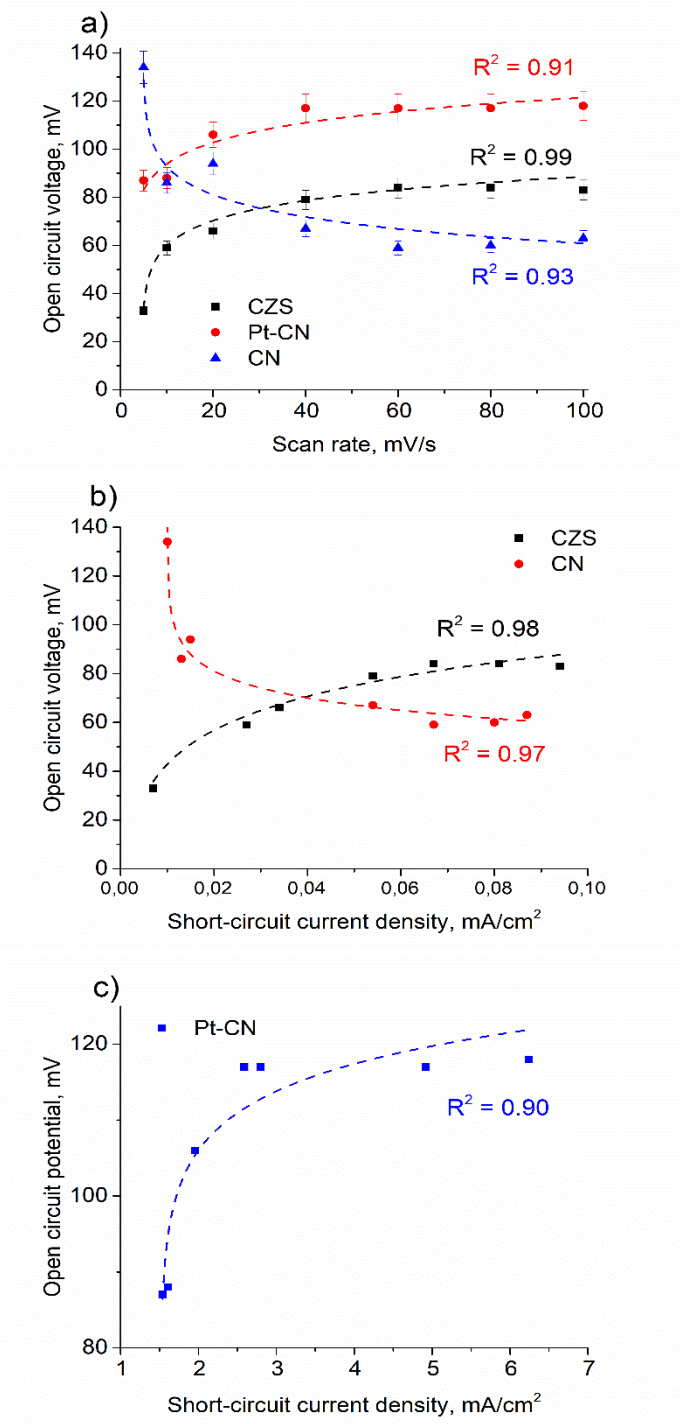

Figure 3 Open-circuit voltage vs a) scan rate; short-circuit current density for the b) CZS and CN, c) Pt-CN The dotted line shows the data approximation by a logarithmic function.

Table 1 – The effect of potential sweep rate on the photogalvanic characteristics.

Scan rate, mV/s	Short-circuit current density, mA/cm²			Open circuit voltage, mV			Fill factor, %			Power conversion efficiency, %		
	CZS	Pt-CN	CN	CZS	Pt-CN	CN	CZS	Pt-CN	CN	CZS	Pt-CN	CN
5	0.007	1.54	0.010	33	87	134	29	24	26	0.001	0.937	0.010
10	0.027	1.61	0.013	59	88	86	24	24	29	0.008	0.983	0.007
20	0.034	1.96	0.015	66	106	94	28	24	28	0.012	1.204	0.008
40	0.054	2.59	0.054	79	117	67	25	26	24	0.022	1.859	0.019
60	0.067	2.80	0.067	84	117	59	28	24	24	0.029	1.711	0.021
80	0.081	4.92	0.080	84	117	60	26	26	25	0.035	2.243	0.026
100	0.094	6.24	0.087	83	118	63	28	26	26	0.040	3.428	0.028

Table 1 shows the dependence of the power conversion efficiency on the scan rate. Like the short-circuit current density, this value grows with the increase of the scan rate for all tested samples. Probably, it is due to the enhancement of reagent concentration near the electrode with the growth of the scan rate. In this case, the rate of electrochemical processes, short-circuit current density, and power conversion efficiency are calculated as the ratio of the maximum possible electrical energy in the cell to the light energy. When the scan rate changes, the main features identified for the short-circuit current density are saved. For example, for CZS and CN samples, the power conversion efficiency in most cases coincides with the experimental error and is 1–2 orders of magnitude lower than for the platinized carbon nitride.

3.2. The effect of the amplitude on the results of impedance spectroscopy

Impedance spectroscopy allows examining the resistivity of the materials and processes occurring at the phase interface and is assigned with the charge carriers transport. The method consists of applying a constant external potential and a potential with variable frequency and amplitude to the photoelectrochemical cell. As a result, an alternating current, which shifted in the phase relative to the potential, and a resistance called impedance are generated in the cell. The impedance is represented in a complex form that highlights the real and imaginary parts. The obtained dependences of the real and imaginary parts are often presented in two forms, such as the Nyquist plot and the Bode plot. It is interesting to study the dependence of impedance on amplitude and external potential.

The impedance measured at an external potential equal to 200 mV in the photoelectrochemical cell, the amplitude was varied from 5 to 100 mV. The obtained Nyquist plots are shown in Figure 4. Figure 4 shows that for all the photoelectrodes, the hodographs consisted of two semicircles slightly shifted with respect to the origin.

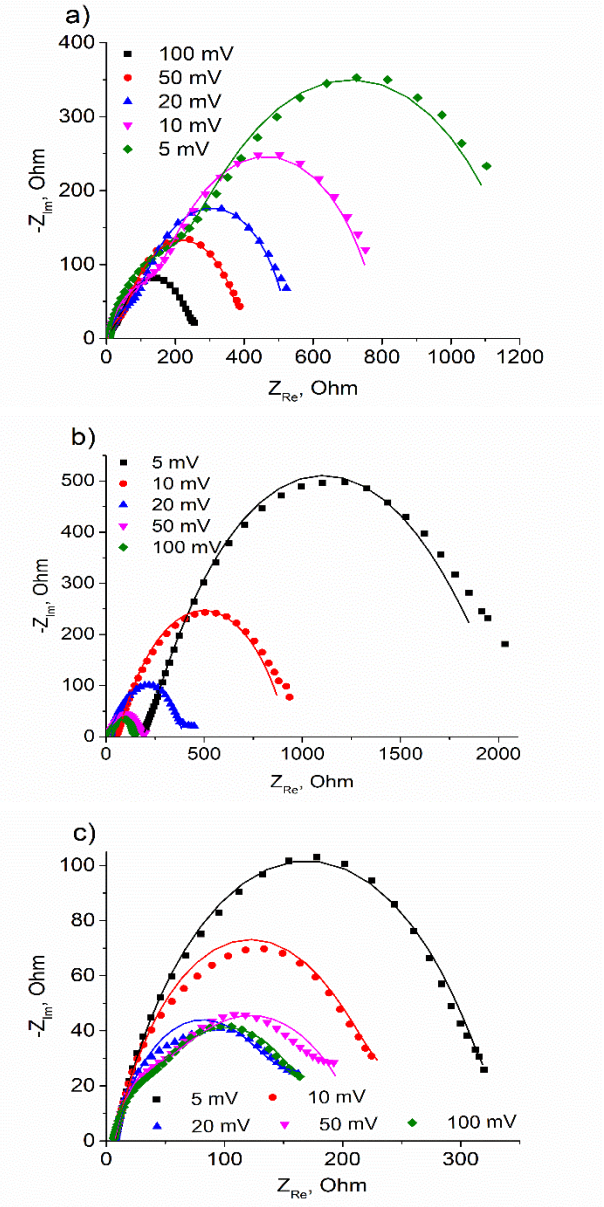

Figure 4 Nyquist plots obtained for the photoelectrochemical cell in the presence of a) CZS; b) CN; c) Pt-CN photoelectrodes.

These curves are often approximated by the equivalent electrical circuit shown in Figure 5. This

circuit consists of a constant resistance and two sequentially connected R-C fragments describing a double electric layer at the phase interface [19–24]. The constant resistance determines the displacement of the first point of the plot relative to the origin. Figure 4 shows that the hodograph shape is preserved with the amplitude changing while the total resistivity is decreased. In the case of Pt-CN, the resistivity obtained at different amplitudes 20–100 mV is the same.

Earlier, the trend to resistivity declining with the amplitude growth was found to the electrochemical hydrogen production [25]. For the electrode coated with carbon nanofibers and immersed in a solution containing ferrous and ferric salts, the same result was observed [26]. In this case, the resistivity decreased with the amplitude growth from 10 to 50 mV. Probably, it was caused by the increase of the maximum value of the generated alternating current under the amplitude growth, which leads to the decrease of the resistance in the photoelectrochemical cell.

The main trends in the change of the system resistance with varying amplitude are reflected in the model parameters approximating experimental data with the equivalent electrical circuit shown in Figure 5. The obtained parameters for the cells with different tested working electrodes are given in Table 2–4.

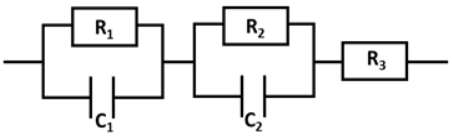

Figure 5 An electrical equivalent circuit used for impedance fitting of the experimental data.

Table 2 – Parameters of the equivalent circuit elements obtained by the approximation of the experimental data and the lifetimes of charge carriers measured in the presence of the CZS photoelectrode.

Amplitude, mV	R_1, Ohm	R_2, Ohm	R_3, Ohm	τ_1, ms	τ_2, ms
5	1034 ± 16	195 ± 8	7.7 ± 0.1	21 ± 4	0.06 ± 0.03
10	654 ± 5	137 ± 3	6.4 ± 0.1	12 ± 4	0.06 ± 0.03
20	439 ± 2	86 ± 2	5.5 ± 0.1	8 ± 2	0.06 ± 0.03
50	343 ± 2	46.5 ± 0.8	5.1 ± 0.1	7 ± 2	0.06 ± 0.03
100	216 ± 1	28 ± 1	4.8 ± 0.1	5 ± 2	0.06 ± 0.03

Table 3 – Parameters of the equivalent circuit elements obtained by the approximation of the experimental data and the lifetimes of charge carriers measured in the presence of the CN photoelectrode.

Amplitude, mV	R_1, Ohm	R_2, Ohm	R_3, Ohm	τ_1, ms	τ_2, ms
5	1375 ± 111	565 ± 116	185 ± 21	2.5 ± 0.9	0.2 ± 0.1
10	841 ± 124	340 ± 24	654 ± 7	1.0 ± 0.5	0.04 ± 0.03
20	372 ± 25	89 ± 6	19 ± 2	1.3 ± 0.4	0.10 ± 0.07
50	164 ± 11	43 ± 4	15 ± 1	1.2 ± 0.6	0.04 ± 0.03
100	133 ± 8	27 ± 6	13 ± 1	1.6 ± 0.7	0.05 ± 0.04

Table 4 – Parameters of the equivalent circuit elements obtained by the approximation of the experimental data and the lifetimes of charge carriers measured in the presence of the Pt-CN photoelectrode.

Amplitude, mV	R_1, Ohm	R_2, Ohm	R_3, Ohm	τ_1, ms	τ_2, ms
5	108 ± 3	324 ± 3	7.3 ± 0.1	4 ± 1	0.3 ± 0.2
10	165 ± 21	212 ± 4	6.8 ± 0.1	4 ± 1	0.2 ± 0.1
20	100 ± 15	71 ± 9	6.6 ± 0.1	4 ± 1	0.14 ± 0.09
50	190 ± 3	23 ± 2	6.3 ± 0.1	5 ± 2	0.12 ± 0.09
100	167 ± 1	14 ± 1	5.8 ± 0.1	5 ± 2	0.12 ± 0.09

Tables 2–4 show that the resistivities, except the parameter R_1 in the case of Pt-CN, decline with the increase of the amplitude. The more interesting task is to compare the approximation parameters at the fixed amplitude. Tables 2–4 show that at the amplitude of 5 and 10 mV all parameters (R_1, R_2, R_3) grow in the transition from the solid solution of CdS and ZnS to carbon nitride and decrease in transition to the platinized sample. When the impedance was measured at different amplitudes 20–100 mV, the trend was found

only for the parameter R_3. The parameters R_2 for the solid solution of CdS and ZnS and carbon nitride obtained at the mentioned amplitudes are the same and exceed the similar value for Pt-CN. The parameter R_1 calculated at all amplitudes decreases for the transition from the solid solution $Cd_{0.8}Zn_{0.2}S$ to g-C_3N_4. The transition to the platinized carbon nitride is accompanied by resistance growth at 50 and 100 mV and resistance declining at 20 mV. Therefore, it should be noted that the behavior of the photoelectrochemical system varies at different amplitudes; however, there are the same features within some groups of amplitudes. To sum up, the comparison of the obtained values may be carried out at various amplitudes that are not very different from each other. It is desirable to compare experimental data at higher amplitude values, since the generated voltage and current are higher, which means that the accuracy of the obtained data will be more appreciable.

Another way to interpret impedance spectroscopy results is to use Bode plots. The x-axis is the logarithm of the frequency to the base 10, while the y-axis is the minus phase shift occurring between the alternating current and the potential. The obtained plots are given in Figure 6. Figure 6 reveals that for all samples, the experimental curve can be presented as the superposition of two curves with one maximum. This fact coincides with the Nyquist plots. There are two hodographs on the Nyquist plots which correspond to neither two different types of the charge carrier or two different processes of the charge transport. The increase in the amplitude leads to the shift of a peak position and its intensity; however, no trends are found.

Knowing the position of the peak maximum on the Bode curve, it is possible to calculate the lifetime of charge carriers by the formula (2).

$$\tau = \frac{1}{2\pi f} \qquad (2)$$

where τ is the electron lifetime, f is the frequency at which the maximum phase shift between alternating voltage and current is observed.

The curves shown in Figure 6 were decomposed into two peaks, from the positions of the maxima of which the lifetime of charge carriers was calculated. The obtained data are given in Tables 2–4. Tables 2–4 show that the electron lifetime measured at 5 mV is slightly higher than those calculated at other amplitudes. In case of amplitudes 10–100 mV, the electron lifetime was the same within the experimental error. To sum up, for the studied samples, the experimental data obtained at different amplitudes can be compared when considering

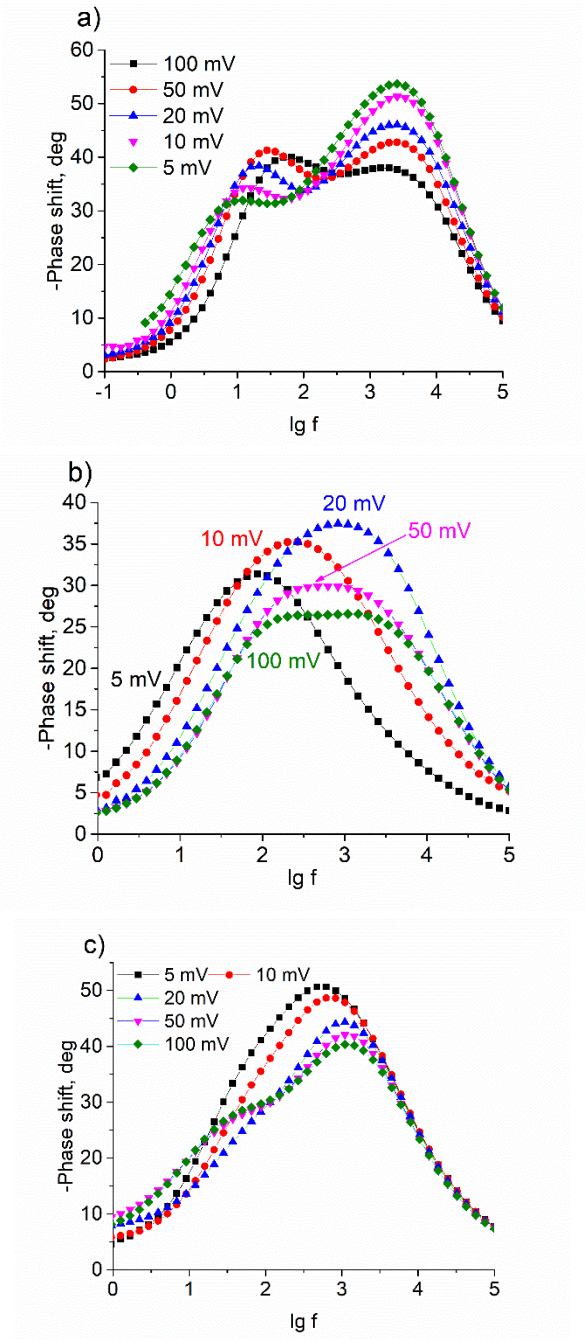

Figure 6 The Bode plots obtained for the photoelectrochemical cell when the working electrode was a) CZS; b) CN; c) Pt-CN.

the lifetimes of the photogenerated charge carriers.

3.3. Effect of external potential on the impedance spectroscopy results

The same experiments in which the resistance was measured were conducted at the amplitude in 10 mV at different external potentials. The results are summarized in Figure 7. It should be noted that for all the photoelectrodes, the shape of hodographs is saved varying the external potential. In all cases, the hodographs consist of two semicircles slightly shifted to the right from the origin, corresponding to a constant resistance and two R-C chains, respectively. The

experimental data were approximated by the equivalent electrical circuit given in Figure 5, and the approximation parameters are summarized in Table 5. For the cells, in which carbon nitride or the solid solution $Cd_{0.8}Zn_{0.2}S$ served as the working electrode, the typical resistances R_1, R_2, and R_3 increase with declining of the external potential from 0.8 V to 0.2 V and decrease with changing the external potential from –0.2 V to –0.8 V. In the case of the platinized carbon nitride, R_1, R_2, and R_3 grow with decreasing of the external potential from 0.8 V to 0 V and go through a maximum at –0.4 V with further falling of the external potential from 0 V to –0.8 V. To evaluate the obtained results, we can use the resistance R^* calculated from the cyclic voltammetry curve according to Ohm's law. The values of R^* are given in Table 5. It should be noted that the features of the change of the resistance R^* from the external potential coincide with those in the parameters of the equivalent electrical circuit R_1, R_2 and R_3 for each of the samples. Thus, the impedance spectroscopy data are consistent with the cyclic voltammetry data.

In the literature, there are various data about the effect of the external potential on the results of impedance spectroscopy. In the case of ZnS deposited on ITO, resistivity decreases with the growth of the external potential from 0 to 1 V [27]. The composite catalyst consisting of titania and graphene oxide demonstrates the same properties: the radii of the hodographs decrease with the increase of the external potential from 0 to 0.5 V [28]. In the photoelectrochemical cell with tin oxide serving as the working electrode contradictory trends are observed [29]. The radii of the hodographs decrease when the external potential changes from 0.8 V to 1.0 V; after that, the increase of the external potential by 0.1 V is accompanied by the growth of the cell resistance. For Gd doped by Ce and deposited on $Pt/TiO_2/SiO_2/Si$, the increase of the external potential from 0 V to 1 V leads to the growth of the hodograph radii, but the further increase of the external potential to 2 V is accompanied by the decrease of the hodograph radii and the changes of the shape of the Nyquist plot [30]. The growth of the external potential to 3 V leads to the decrease of the semicircle radii [30]. By the way, the general dependences of the impedance on the external potential are not found, they are individual and depend on the photoelectrode nature.

An important issue is the comparison of the resistance values of all samples at the fixed external potential. In our experiments, the same dependences of the approximation parameters on the external potential are observed in the range of –0.4 V to 0.8 V. In these cases, the resistances decrease in the transition from CN or CZS to Pt-CN. Thus, in a wide range of potentials, qualitative features of impedance changes remain depending on the sample nature. Accordingly, in this range of external potentials, samples can be correctly compared with each other.

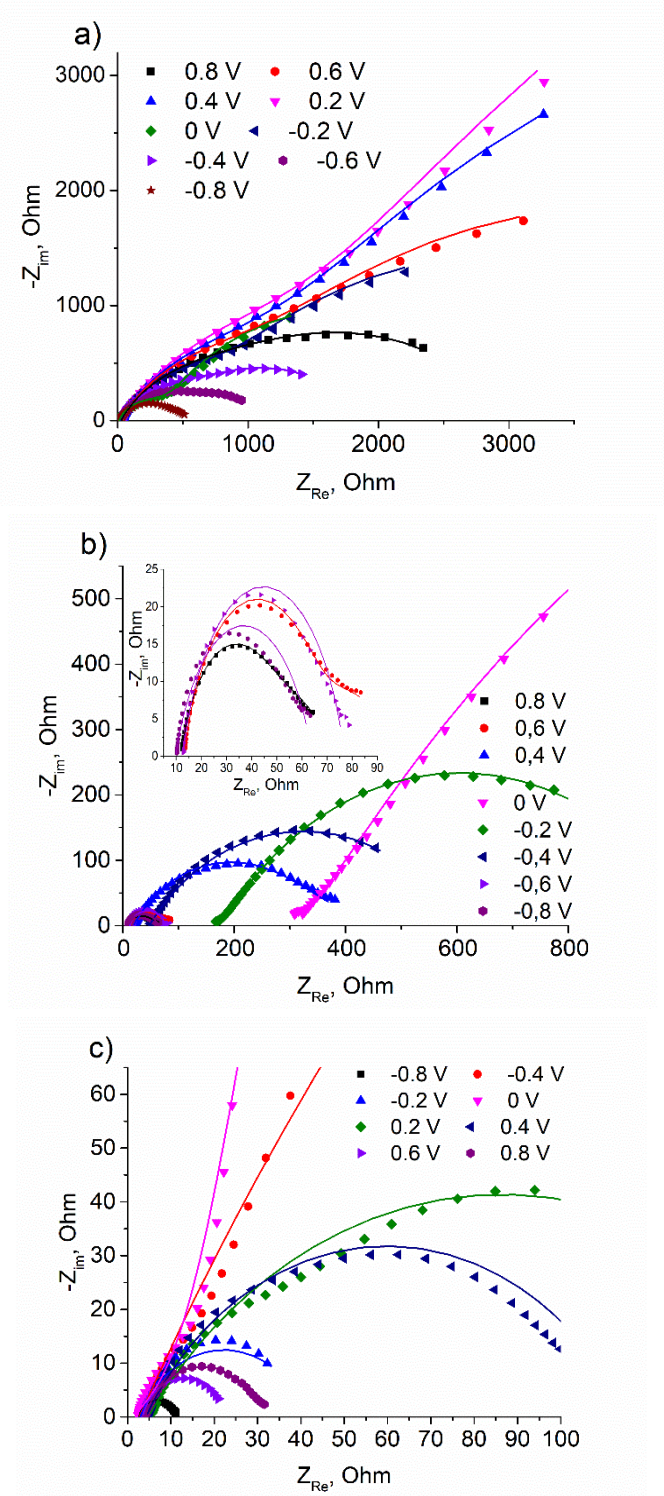

Figure 7 The Bode plots obtained for the photoelectrochemical cell when the working electrode was a) CZS; b) CN; c) Pt-CN.

Table 5 – The effect of the external potential on the approximation parameters and the constant resistance calculated from the CVA data.

External potential, V	R^*, Ohm			R_1, Ohm			R_2, Ohm			R_3, Ohm		
	CZS	CN	Pt-CN	CZS	CN	Pt-CN	CZS	CN	Pt-CN	CZS	CN	Pt-CN
0.8	426	78	126	(2.1 ± 0.2)·10³	26 ± 5	44 ± 8	368 ± 12	12 ± 2	19 ± 1	16 ± 1	20 ± 1	3.4 ± 0.2
0.6	673	100	149	(5.8 ± 0.3)·10³	32 ± 7	89 ± 13	533 ± 20	34 ± 4	46 ± 4	20 ± 1	14 ± 1	4.1 ± 0.3
0.4	932	152	170	(12 ± 1)·10³	69 ± 8	111 ± 2	595 ± 39	52 ± 7	104 ± 21	24 ± 1	12 ± 1	4.2 ± 0.2
0.2	1869	403	298	(19.5 ± 0.4)·10³	439 ± 2	163 ± 15	722 ± 73	86 ± 2	212 ± 4	27 ± 1	5.5 ± 0.1	6.8 ± 0.1
0	0	0	0	2797 ± 28	350 ± 12	1782 ± 319	352 ± 12	502 ± 56	450 ± 29	11 ± 1	29 ± 1	7.2 ± 0.8
–0.2	1754	403	100	(4.4 ± 0.1)·10³	824 ± 7	115 ± 23	1413 ± 75	247 ± 79	39 ± 3	31 ± 2	9.6 ± 0.8	2.7 ± 0.1
–0.4	1325	364	113	1215 ± 50	646 ± 12	757 ± 27	1141 ± 110	189 ± 24	94 ± 17	30 ± 1	6.5 ± 0.3	2.89 ± 0.01
–0.6	1279	249	101	533 ± 24	554 ± 29	128 ± 12	1023 ± 114	124 ± 37	59 ± 8	29 ± 1	4.2 ± 0.3	2.64 ± 0.01
–0.8	1205	159	90	169 ± 1	364 ± 16	16 ± 6	823 ± 77	49 ± 8	17 ± 2	28 ± 1	2.2 ± 0.1	2.21 ± 0.08

Table 6 – Electron lifetimes measured in the cells with the CZS, CN, and Pt-CN photoelectrodes with varying the external potential.

External potential, V	τ_1, ms			τ_2, ms		
	CZS	CN	Pt-CN	CZS	CN	Pt-CN
0.8	11 ± 3	1.1 ± 0.3	0.06 ± 0.03	0.2 ± 0.1	0.05 ± 0.02	0.25 ± 0.09
0.6	14 ± 3	6 ± 1	0.05 ± 0.02	0.2 ± 0.1	0.05 ± 0.02	0.16 ± 0.06
0.4	32 ± 6	0.6 ± 0.2	0.11 ± 0.06	0.4 ± 0.2	0.06 ± 0.02	2 ± 1
0.2	80 ± 6	0.04 ± 0.03	0.12 ± 0.07	0.3 ± 0.1	49 ± 0.5	4 ± 1
0	48 ± 6	4.3 ± 0.7	0.2 ± 0.1	0.09 ± 0.06	0.05 ± 0.02	0.6 ± 0.3
–0.2	56 ± 6	7 ± 1	8 ± 1	0.4 ± 0.2	0.09 ± 0.03	0.007 ± 0.003
–0.4	10 ± 3	1.1 ± 0.3	1.2 ± 0.5	0.2 ± 0.1	0.04 ± 0.01	27 ± 5
–0.6	7 ± 2	7 ± 1	0.6 ± 0.2	0.2 ± 0.1	0.19 ± 0.06	11 ± 3
–0.8	5 ± 2	0.19 ± 0.06	0.2 ± 0.1	0.2 ± 0.1	0.14 ± 0.05	0.3 ± 0.1

Figure 8 shows the impedance results in the Bode coordinates. For all samples, the changes in the external potential leads to different changes in the peak positions. The slight change in the peak position was found for the cell with $Cd_{0.8}Zn_{0.2}S$. For carbon nitride, the position of the peak maximum is shifted by a higher value, while for Pt-CN there are no features.

All Bode plots are the superposition of two curves. The peaks were decomposed into two components, and the lifetime of charge carriers was calculated from the obtained values. All calculated values are given in Table 6. For CZS, electron lifetimes decline with the decrease of the external potential from 0.8 V to 0.2 V and from -0.2 V to –0.8 V. In case of graphitic carbon nitride, for the first type of charge carriers no features are found, while for the second type the electron lifetimes are the same within the experimental error with the declining external value. For Pt-CN no features are observed. It is noteworthy that in the case of the fixed external potential, there are different trends in changing lifetimes. For the first type of charge carriers, at all potentials different from 0.2 V, –0.2 V, –0.4 V and –0.8 V, the lifetime decreases with the transition from the solid solution of cadmium sulfide and zinc sulfide to carbon nitride and platinized carbon nitride. For the second type of charge carriers in the same row, the lifetimes go through the minimum at the potentials of 0.4–0.8 V, 0 V and –0.4 V.

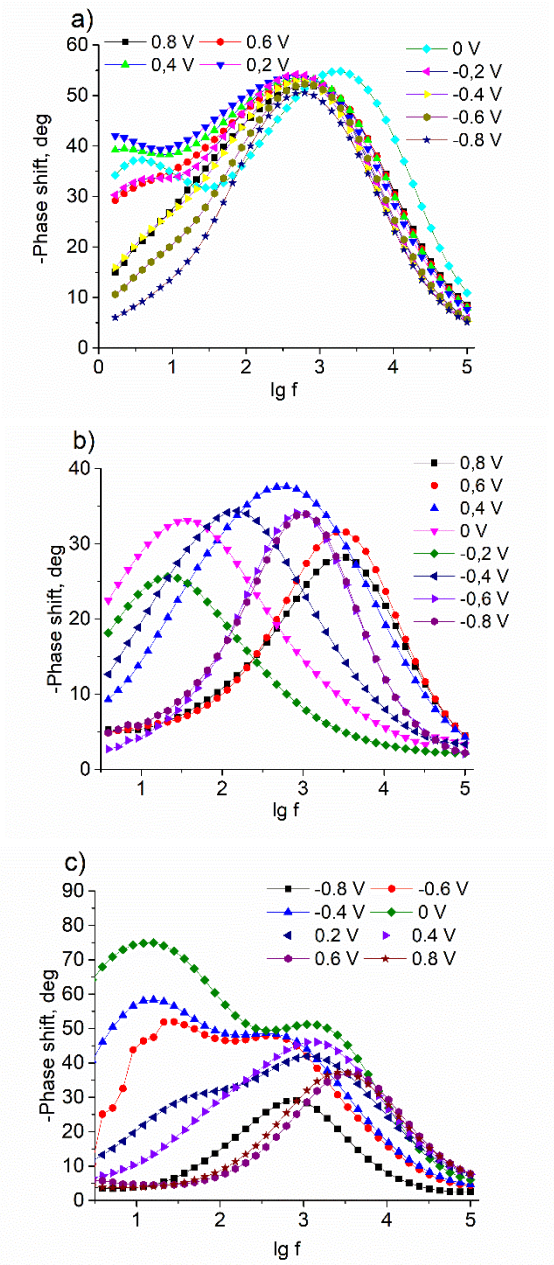

Figure 8 The Bode plots obtained for the cell in which a) CZS; b) CN; c) Pt-CN are the working electrodes.

The obtained results in the Bode plots show that the external potential is crucial for the electrochemical properties of the studied systems. It is possible to compare the obtained electrochemical data with each other only in relation to the shape of the hodographs (the type of equivalent electrical circuit) and the number of types of charge carriers that differ in electrochemical properties.

3.4. The effect of the frequency on the number of charge carriers and the flat-band potential calculated from the Mott–Schottky plots

The Mott – Schottky analysis studies the phase interface between the semiconductor and the electrolyte. The equalization of the electrochemical potential and the

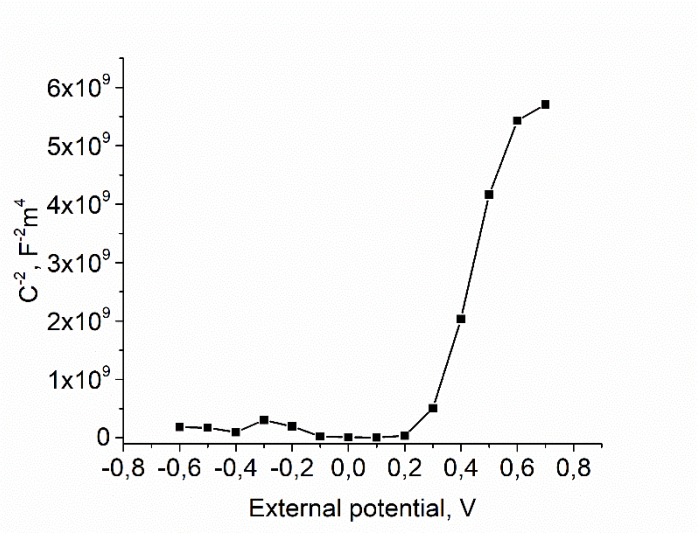

Figure 9 The Mott – Schottky plot obtained for the photoelectrochemical cell with carbon nitride as the working electrode at 100 Hz.

diffusion of charges arising from the contact of the semiconductor with an electrolyte solution leads to the formation of a depleted layer with an electrical capacity. This capacitance can be calculated by obtaining impedance hodographs at different potentials and knowing the model of an equivalent electrical circuit that approximate experimental data. [10]. At the fixed frequency, the dependences of C^{-2} on the applied potential were plotted. Figure 9 shows the typical Mott – Schottky plot obtained for CN and Pt-CN. Directly from the graph, one can determine the type of conductivity of the analyzed sample. In our case, the linear part of the graph has a positive slope, which indicates the hole conductivity of carbon nitride and is consistent with literature data [31–34].

In the experiments, the Mott – Schottky dependences at different frequencies (lg(*f*) = 0–5) were studied. For the tested electrodes, there is one linear part on the experimental curve at all frequencies. The obtained result allows one to add impedance spectroscopy results. Two found hodographs are attributed to different electron transport processes (e.g., at the working electrode/electrolyte or the counter electrode/electrolyte interfaces) and not to two different charge carrier types.

At the qualitative level, Mott – Schottky plots allows calculating the flat-band potential and evaluating amount of charge carriers. For this purpose, the linear part of the plot is chosen, after which these data are fitted according to the following formula for p-type semiconductors [35]:

$$\frac{1}{C^2} = \frac{2}{\varepsilon \cdot \varepsilon_0 \cdot N \cdot A^2 \cdot e}\left(-E + V_{FB} - \frac{k_B \cdot T}{e}\right) \qquad (3)$$

Table 7 – The dependences of the flat-band position and density of charge carriers on the frequency.

Frequency, Hz	Flat-band potential, V		Densities of charge carriers, m^{-3}	
	CN	Pt-CN	CN	Pt-CN
10^5	0.61 ± 0.05	0.6 ± 0.2	(8 ± 1)·10^{15}	(1.2 ± 0.1)·10^{13}
10^4	0.7 ± 0.1	0.88 ± 0.09	(2.6 ± 0.2)·10^{19}	(3.1 ± 0.4)·10^{16}
10^3	0.30 ± 0.02	0.17 ± 0.04	(7.3 ± 0.8)·10^{19}	(3.9 ± 0.4)·10^{19}
10^2	0.36 ± 0.07	0.19 ± 0.03	(1.1 ± 0.1)·10^{20}	(6.8 ± 0.5)·10^{19}
10	0.38 ± 0.02	0.15 ± 0.02	(2.7 ± 0.2)·10^{20}	(1.7 ± 0.3)·10^{21}
1	0.34 ± 0.02	0.21 ± 0.07	(2.9 ± 0.7)·10^{21}	(2.4 ± 0.6)·10^{21}

where C is the capacity of the depleted charge area (F), ε is the dielectric constant of the photocatalyst, ε_0 is the permittivity of vacuum (F/m), N is the density of charge carriers (m^{-3}), A is the irradiation surface (m^2), e is the electron charge (C), E is the applied potential (V), V_{FB} is the flat-band potential (V), k_B is the Boltzmann constant (J/K), T is the temperature (K). The flat-band position is calculated from the ratio of the intercept to the slope, the amount of charge carriers is evaluated from the slope. The mentioned values were calculated for the photoelectrochemical cell with carbon nitride or the platinized carbon nitride and are given in Table 7.

From the literature, it is known that flat-band potentials are weakly dependent on frequency when the frequencies are of the same order of magnitude [31, 35–37]. For example, V_{fb} of GaP is about 0.8 V in aqueous solution of sulfuric acid (pH = 1) at frequencies 1–15 kHz [35]. For Ti_3SiC_2 treated with hydrochloric acid, the flat-band potential did not change at frequencies 100 – 1000 Hz [36]. For titania thin films, the change in the frequency leads to a slight shift of the flat-band potential (0.06–0.1 V) due to the experimental errors [36]. The V_{fb} for the platinized carbon nitride in sodium sulfate was –1.31 V at 500–1500 Hz [37]. In our experiments, for both samples two different values at 10^4–10^5 Hz (0.6 V for CN, 0.9 V for Pt-CN) and 1-1000 Hz (0.3 V for CN and 0.2 V for Pt-CN) are observed. Probably, it is due to different types of charge transfer that the mechanism of depleted charge area formation and its capacity is realized at varied frequencies. Moreover, the found trends depend on the frequency range. At high frequencies, V_{fb} of carbon nitride is higher than that of the platinized sample, while at low frequencies the opposite trend is observed.

Another important characteristic of the semiconductor calculated from the Mott – Schottky plot was charge densities. This parameter was evaluated for the slop (see Equation (4)), the obtained values are given in Table 7.

$$N = \frac{-2}{\varepsilon \cdot \varepsilon_0 \cdot \alpha \cdot A^2 \cdot e} \qquad (4)$$

where N is the charge density (m^{-3}), ε is the dielectric constant of the photocatalyst, ε_0 is the permittivity of vacuum (F/m), α is the slope, A is the surface of the irradiation (m^2), e is the electron charge (C).

Table 7 shows that at 1 Hz the charge densities for both samples are the same within the experimental error. The increase in the frequency leads to the declining of charge carrier amounts for both samples. The observed trend is depicted in the growth of the slope and C^{-2} at whole. This observation coincides with the literature data: the increase in frequency leads to the growth of values of C^{-2} [31, 35–39]. The results obtained at higher frequencies are more reliable, because in these cases the part of the surface sites in the capacity is minimal [10]. It should be noted that for the studied samples charge densities in CN were higher than in Pt-CN at frequencies higher than 100 Hz. To sum up, the comparison of charge amounts can be conducted at higher frequencies.

4. Conclusions

In this work, the photoelectrochemical properties of the solid solution of CdS and ZnS, carbon nitride, and platinized carbon nitride were studied under different experimental conditions. The photoelectrodes are tested by cyclic voltammetry at varied scan rates from 5 to 100 mV/s. At the quantitative level, the behavior of the voltammograms does not change with varying scan rate. The photoelectrodes are better to study at low scan rates, where the differences between the electrochemical activities are more evident. Additionally, the changes in the photovoltaic parameters are studied. The short-circuit current densities increase in proportion to the square root of the potential scan rate. The open circuit potential changes according to the logarithmic law with the growth of the scan rate and reaches a plateau. The fill factor practically does not depend on the scan rate. The power conversion efficiency grows with the increase of the scan rate for all tested samples. The impedance spectroscopy study was performed in two ways, at the external potential of 200 mV and different amplitudes, and at an amplitude of 10 mV and different external

potentials. In all cases, the shapes of hodographs forms are the same. The hodographs radii decrease with increasing the amplitude. The correct comparison of the data depicted in the Nyquist plots can be realized at different amplitudes that are closer to each other. The electron lifetime calculated from the Bode plots can be compared at all amplitudes. In the case of experiments with varying values of the external potential, it is difficult to identify clear features of changes in resistance values for a particular sample. The qualitative features of the impedance changes remain over a wide range of potentials, depending on the nature of the samples, and over this range of potentials it is possible to correctly compare the quantitative data shown on the Nyquist plots. However, the electron lifetime is difficult to compare, as these values are too sensitive to the external potential. The Mott – Schottky method is the important one that characterizes the properties of semiconductor photocatalysts. These experiments were carried out at different frequencies. It has been shown that it is correct to compare the flat-band potentials obtained at different frequencies only in a narrow frequency range. In the case of estimating the number of charge carriers, the qualitative patterns differ at high and low frequencies. It is recommended to compare the data in the high frequency region, where extraneous contributions to the depleted layer capacity are minimal. In the future, the tested samples will be studied at different electrolytes under the optimized electrochemical conditions reached in this work. Also, we plan to expand the nature of the tested photoelectrodes. Further investigation allows researchers to compare the experimental data with each other more competently.

Supplementary materials

No supplementary materials are available.

Funding

This work was supported by the Russian Science Foundation (RSF grant No 21–13–00314).

Acknowledgments

None.

Author contributions

Dina Markovskaya: Conceptualization; Data curation; Formal Analysis; Methodology; Project administration; Software; Visualization; Writing – original draft; Writing – review & editing.

Nikolay Sidorenko: Data curation; Investigation; Validation.

Angelina Zhurenok: Investigation; Validation.

Ekaterina Kozlova: Conceptualization; Funding acquisition; Supervision; Resources; Writing – review & editing.

Conflict of interest

The authors declare no conflict of interest.

Additional information

Author IDs:
Dina V. Markovskaya, Scopus ID 55895307200.
Angelina V. Zhurenok, Scopus ID 57213824739.
Ekaterina A. Kozlova, Scopus ID 12244601300.
Website:
Boreskov Institute of Catalysis, https://catalysis.ru.

References

1. Gao W, Zhang S, Wang G, Cui J, et al. A review on mechanism, applications and influencing factors of carbon quantum dots based photocatalysis, Ceram. Int. **48** (2022) 35986–35999. https://doi.org/10.1016/j.ceramint.2022.10.116

2. Wudil YS, Ahmad UF, Gondal MA, Mohammed AA-O, et al. Tuning of graphitic carbon nitride (g-C3N4) for photocatalysis: A critical review, Arab. J. Chem. **16** (2023) 104542. https://doi.org/10.1016/j.arabjc.2023.104542

3. Sun L, Han L, Huang J, Luo X, et al. Single-atom catalysts for photocatalytic hydrogen evolution: A review, Int. J. Hydrogen Energy. **47** (2022) 17583–17599. https://doi.org/10.1016/j.ijhydene.2022.03.259

4. Pachaiappan R, Rajendran S, Kumar PS, Vo D-VN, et al. A review of recent progress on photocatalytic carbon dioxide reduction into sustainable energy products using carbon nitride, Chem. Eng. Res. Des. **177** (2022) 304–320. https://doi.org/10.1016/j.cherd.2021.11.006

5. Wang Z, Zhang Z, Wang Z, Lu H, et al. Can we achieve efficient photocatalytic partial oxidation of methane to methanol: A perspective on oxygen reaction pathways, Appl. Catal. A-Gen. **654** (2023) 119082. https://doi.org/10.1016/j.apcata.2023.119082

6. Feng Y, Su X, Chen Y, Liu Y, Zhao X, et al. Research progress of graphene oxide-based magnetic composites in adsorption and photocatalytic degradation of pollutants: A review, Mater. Res. Bull. **162** (2023) 112207. https://doi.org/10.1016/j.materresbull.2023.112207

7. Ollis DF. Photocatalytic purification and remediation of contaminated air and water, Surf. Chem. Cat. **3** (2000) 405–411. https://doi.org/10.1016/S1387-1609(00)01169-5

8. Helali S, Polo-López MI, Fernández-Ibáñez P, Ohtani B, et al. Solar photocatalysis: A green technology for E. coli contaminated water disinfection. Effect of concentration and different types of suspended catalyst, J. Photochem. Photobiol. A. **276** (2014) 31–40. https://doi.org/10.1016/j.jphotochem.2013.11.011

9. Kamat PV, Tvrdy K, Baker DR, Padich JG Beyong photovoltaics: semiconductor nanoarchitectures for liquid-junction solar cells, Chem. Rev. **110** (2010) 6664–6688. https://doi.org/10.1021/cr100243p

10. Gurevich YY, Pleskov YV. Photoelectrochemistry of semiconductors [Photoelektrohimiya poluprovodnikov]. Moscow: Nauka; 1983. 312 p. Russian.

11. Senthil V, Badapanda T, Chithambararaj A, Bose AC, Panigrahi S Impedance spectroscopy and photocatalysis water splitting for hydrogen production with cerium modified SrBi2Ta2O9 ferroelectrics, Int. J. Hydrogen Energy. **41** (2016) 22856–22865. https://doi.org/10.1016/j.ijhydene.2016.08.139

12. Cui RC, Wang YF, Li Z, Zhou L, et al. Micrometer-sized fluorine doped tin oxide as fast electron collector for enhanced dye-sensitized solar cells, ACS Appl. Mater. Interfaces. **6** (2014) 16593–16600. https://doi.org/10.1021/am503074j

13. Bai P, Wang P, Li T, Jing J, et al. Alkali functionalized carbon nitride with internal van der Waals heterostructures: Directional charge flow to enhance photocatalytic hydrogen production, J. Colloid Interface Sci. **644** (2023) 211–220; https://doi.org/10.1016/j.jcis.2023.04.087

14. Chen H, Mo Z, Wang Z, Yan P, et al. Implanting nitrogen-doped graphene quantum dots on porous ultrathin carbon nitride for efficient metal-free photocatalytic hydrogen evolution,J. Environ. Chem. Eng. **11** (2023) 109801; https://doi.org/10.1016/j.jece.2023.109801

15. Markovskaya DV, Zhurenok AV, Cherepanova SV, Kozlova EA, et al. Solid Solutions of CdS and ZnS: Comparing Photocatalytic Activity and Photocurrent Generation, Appl. Surf. Sci. Adv. **4** (2021) 100076:1–8. https://doi.org/10.1016/j.apsadv.2021.100076

16. Zhurenok AV, Larina TV, Markovskaya DV, Cherepanova SV, et al. Synthesis of Graphitic Carbon Nitride-Based Photocatalysts for Hydrogen Evolution Under Visible Light, Mendeleev Commun. **31** (2021) 157–159. https://doi.org/10.1016/j.mencom.2021.03.004

17. Hassan M, Gondal MA, Cevik E, Dastageer MA. Laser assisted anchoring of cadmium sulfide nanospheres into tungsten oxide nanosheets for enhanced photocatalytic and electrochemical energy storage applications, Colloids and Surfaces A: Physicochemical and Engineering Aspects. **617** (2021) 126318. https://doi.org/10.1016/j.colsurfa.2021.126318

18. Cheng C, Shi J, Mao L, Dong C-L, et al. Ultrathin porous graphitic carbon nitride from recrystallized precursor toward significantly enhanced photocatalytic water splitting, J. Colloid Interface Sci. **637** (2023) 271–282. https://doi.org/10.1016/j.jcis.2023.01.098

19. Wu Q, Hou J, Zhao H, Liu Z, et al. Charge recombination control for high efficiency CdS/CdSe quantum dot co-sensitized solar cells with multi-ZnS layers, Dalton T. **47** (2018) 2214–2221. https://doi.org/10.1039/c7dt04356b

20. Jun HK, Careem MA, Arof AK. Performances of some low-cost counter electrode materials in CdS and CdSe quantum dot-sensitized solar cells, Nanoscale Res. Lett. **9** (2014) 69. https://doi.org/10.1186/1556-276X-9-69

21. Shinde DV, Ahn DY, Jadhav VV, Lee DE, et al. A coordination chemistry approach for shape controlled synthesis of indium oxide nanostructures and their photoelectrochemical properties, J. Mater. Chem. A. **2** (2014) 5490–5498. https://doi.org/10.1039/C3TA15407F

22. Li H, Yu Q, Huang Y, Yu C, et al. Ultralong Rutile TiO2 Nanowire Arrays for Highly Efficient Dye-Sensitized Solar Cells, ACS Appl. Mater. Interfaces **8** (2016) 13384–13391. https://doi.org/10.1021/acsami.6b01508

23. Tian J, Lv L, Fei C, Wang Y, et al. A highly efficient (>6%) Cd1−xMnxSe quantum dot sensitized solar cell, J. Mater. Chem. A. **2** (2014) 19653–19659. https://doi.org/10.1039/C4TA04534C

24. Lee S, Price KJ, Kim D-H. Two local built-in potentials of H2S processed CZTSSe by complex impedance spectroscopy, Sol. Energy. **225** (2021) 11–18. https://doi.org/10.1016/j.solener.2021.06.064

25. Harrington DA. Theory of electrochemical impedance of surface reaction: second-harmonic and large-amplitude response, Can. J. Chem. **75** (1997) 1508–1517. https://doi.org/10.1139/v97-181

26. Siddiqui S, Arumugam PU, Chen H, Li J, et al. Characterization of Carbon Nanofiber Electrode Arrays Using Electrochemical Impedance Spectroscopy: Effect of Scaling Down Electrode Size, ACS Nano **4** (2010) 955–961. https://doi.org/10.1021/nn901583u

27. Dey A, Dhar J, Sil S., et al. Bias Voltage-Dependent Impedance Spectroscopy Analysis of Hydrothermally Synthesized ZnS. Nanoparticles, J. of Materi Eng and Perform. **27** (2018) 2727–2733. https://doi.org/10.1007/s11665-018-3359-x

28. Chakraborty M, Kadir ES, Gayen RN. GO induced grain-boundary modification in transparent TiO2-GO nanocomposite thin films: Study by DC bias dependent impedance spectroscopy, Chem. Phys. Lett. **808** (2022) 140116. https://doi.org/10.1016/j.cplett.2022.140116

29. Ebadi F, Taghavinia N, Mohammadpour R, et al. Origin of apparent light-enhanced and negative capacitance in perovskite solar cells, Nat. Commun. **10** (2019) 1574. https://doi.org/10.1038/s41467-019-09079-z

30. Sulekar SS, Ordonez JE, Arango IC, Gomez ME, Nino JC. Effect of a DC bias on the conductivity of gadolinia doped ceria thin films, Electrochim. Acta. **303** (2019) 275-283. https://doi.org/10.1016/j.electacta.2019.02.073

31. Chen L, Li H, Li H, Li H, et al. Accelerating photogenerated charge kinetics via the g-C3N4 Schottky junction for enhanced visible-light-driven CO2 reduction, Appl. Catal. B-Environ. **318** (2022) 121863. https://doi.org/10.1016/j.apcatb.2022.121863

32. Liu K, Wang X, Li C, Gao M, et al. Facile fabrication metal Cu-decorated g-C3N4 photocatalyst with Schottky barrier for efficient pollutant elimination, Diam. Relat. Mater. **126** (2022) 109116. https://doi.org/10.1016/j.diamond.2022.109116

33. Aboubakr AEA, Khan MD, Revaprasadu N, Millet P, et al. Sn-doped g-C3N4 as a novel photoelectrocatalyst for water oxidation, J. Phys. Chem. Solids. **176** (2023) 111242. https://doi.org/10.1016/j.jpcs.2023.111242

34. Zhao M, Yang X, Li X, Tang Z, et al. Photocathodic protection performance of Ni3S2/g-C3N4 photoanode for 304 stainless steel, J. Electroanal. Chem. **893** (2021) 115324. https://doi.org/10.1016/j.jelechem.2021.115324

35. Gomes WP, Vanmaekelbergh D. Impedance spectroscopy at semiconductor electrodes: review and recent developments, Electrochim. Acta. **41** (1996) 967–973. https://doi.org/10.1016/0013-4686(95)00427-0

36. Jovic VD, Barsoum MW. Corrosion Behavior and Passive Film Characteristics Formed on Ti, Ti3SiC2, and Ti4AlN3 in H2SO4 and HCl, J. Electrochem. Soc. **151** (2004) B71. https://doi.org/10.1149/1.1637897

37. Zhang G, Lan Z-A, Lin L, Lin S, et al. Overall water splitting by Pt/g-C3N4 photocatalysts without using sacrificial agents, Chem. Sci. **7** (2016) 3062–3066. https://doi.org/10.1039/C5SC04572J

38. Ismael M, Wark M. Perovskite-type LaFeO3: Photoelectrochemical Properties and Photocatalytic Degradation of Organic Pollutants Under Visible Light Irradiation, Catalysts. **9** (2019) 342. https://doi.org/10.3390/catal9040342

39. Beranek R. (Photo)electrochemical Methods for the Determination of the Band Edge Positions of TiO2-Based Nanomaterials, Adv. Phys. Chim. **2011** (2011) 1–20. https://doi.org/10.1155/2011/786759